Self-Pinning by Colloids Confined at a Contact Line

Byung Mook Weon* and Jung Ho Je†

X-ray Imaging Center, Department of Materials Science and Engineering, Pohang University of Science and Technology, San 31, Hyoja-dong, Pohang 790-784, Korea

(Received 14 June 2012; published 11 January 2013)

Colloidal particles suspended in a fluid usually inhibit complete wetting of the fluid on a solid surface and cause pinning of the contact line, known as self-pinning. We show differences in spreading and drying behaviors of pure and colloidal droplets using optical and confocal imaging methods. These differences come from spreading inhibition by colloids confined at a contact line. We propose a self-pinning mechanism based on spreading inhibition by colloids. We find a good agreement between the mechanism and the experimental result taken by directly tracking individual colloids near the contact lines of evaporating colloidal droplets.

DOI: 10.1103/PhysRevLett.110.028303 PACS numbers: 47.57.J−, 68.08.Bc, 82.70.Dd, 82.70.Kj

Colloidal fluids including evenly dispersed colloids (colloidal particles or nanoparticles) usually exhibit "self-pinning" on a flat solid surface [1–3], while pure fluids (without solutes) show significant spreading behaviors [4,5]. Nanoparticles in nanofluids can modify spreading dynamics [6]. As commonly seen in coffee stains, self-pinning by solute confinement at a three-phase (liquid-solid-vapor) contact region is an important phenomenon that governs droplet evaporation kinetics and the well-known "coffee-ring" effect [1–3]. Self-pinning by solutes is a basic requisite for the coffee-ring effect and is believed to be driven by surface imperfection [1] or solute accumulation [2]. Generally, a drop of colloid quickly grows to its largest contact radius on a flat solid surface and gets pinned for most of the drying time, which is essentially different from spreading in a pure liquid [2]. Colloidal particles in a fluid are suspected to inhibit spreading dynamics, because a capillary force from colloids confined at a contact line [7–9], which is much stronger than thermal energy, can be a driving force for self-pinning. However, quantitative evidence is still scarce to confirm the role of colloidal particles in self-pinning and the critical conditions in the onset of self-pinning.

In this Letter, we suggest a self-pinning mechanism based on spreading inhibition by colloid confinement at a three-phase contact line and provide quantitative evidence to account for the onset of self-pinning in colloidal fluids. We carefully compare spreading and drying behaviors of pure and colloidal droplets on the same solid surfaces using model colloid systems with optical and confocal imaging methods. The same solid surfaces are useful for ruling out surface imperfection effects on self-pinning so that self-pinning depends only on the presence of colloids. We find a critical linear packing fraction of colloids at a contact line that initiates self-pinning by colloid confinement at very early times. Based on microscopic observations for colloidal droplets with nanoparticles or microparticles, we identify colloid confinement kinetics at a contact line that would critically affect self-pinning.

We monitored spreading and drying behaviors with pure and colloidal droplets using optical microscopy (KSV CAM 101) in Fig. 1(a) and confocal microscopy (Leica TCS SP5) in Fig. 1(b). We compared pure and colloidal droplets on glass surfaces in terms of macroscopic behaviors with optical microscopy. To get insight into the effect of colloidal particles, poly(methyl methacrylate) (PMMA) colloidal particles labeled with a fluorescent dye were used with optical imaging and for tracking of individual particle motions with confocal imaging [8,10]. Each droplet was gently deposited onto a clean cover glass (VWR, 22×30 mm, No. 1.5) in all experiments. As standard solvents in pure and colloidal droplets, we used a mixture of *cis*- and *trans*- decalin (Decahydronaphthalene, ≥99%, Sigma-Aldrich), which is widely used in drying experiments [8,11,12]. The initial drop volume was controlled to be $V_0 \approx 0.5$ μl, resulting in the initial contact radius $R_0 = 1.4$ mm, which is smaller than the capillary length (≈1.9 mm for decalin), and therefore the droplet shape was spherical. The PMMA colloids were stabilized by a thin (10–20 nm) grafted layer of poly(12-hydroxystearic acid), synthesized by A. Schofield [13]. These colloids have little interaction between them and are proper to study the colloid confinement effect on the pinning. The colloid radii were $r_S = 0.1$ μm (small colloids) and $r_L = 1.0$ μm (large colloids) with ∼5% polydispersity in size (determined by dynamic light scattering; ALV 5000, 532 nm laser, 90° scattering angle). The density difference between colloids (1.19 g cm^{-3}) and decalin (0.897 g cm^{-3}) is small enough to prevent any sedimentation issue for microscopic colloids [14].

A droplet of a pure fluid on a solid surface initially spreads to reach a maximum radius and then shrinks by further evaporation [2], as seen in a pure decalin droplet on a glass substrate (Supplemental Material, movie 1 [15]). Interestingly no initial spreading appears in colloidal fluids containing small (particle radius; $r_S = 0.1$ μm, volume fraction; $\phi_S = 1\%$: movie 2 [15]) or large particles

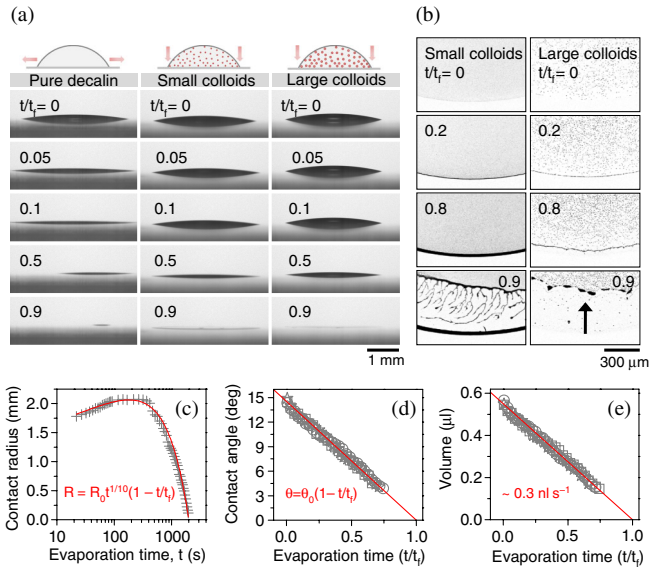

FIG. 1 (color online). Difference in spreading of pure or colloidal droplets on glass surfaces. Spreading and drying behaviors were monitored using (a) optical microscopy (KSV CAM 101) and (b) confocal microscopy (Leica TCS SP5) with time (t) normalized by complete drying time (t_f). For large colloids, the retraction was observed at late times (the arrow). A pure decalin droplet on a clean glass surface initially spreads to reach a maximum contact radius and in turn shrinks by evaporation, while colloidal droplets, including small ($r_S = 0.1$ μm, $\phi_S = 1\%$) or large ($r_L = 1.0$ μm, $\phi_L = 1\%$) particles, rapidly get pinned at very early times. (c) The contact radius for pure decalin droplets shows a typical dynamics as $R(t) = R_0 t^{1/10}(1 - t/t_f)$. (d) The contact angle for colloidal droplets shows a linear decrease as $\theta(t) = \theta_0(1 - t/t_f)$. (e) The droplet volume linearly decreases with time as $V(t) = V_0(1 - t/t_f)$, fitted with $\theta_0 \approx 15°$, $V_0 \approx 0.5$ μl, and $t_f \approx 1700$ s. The linear decreases in $\theta(t)$ and $V(t)$ corroborate self-pinning, regardless of the particle size ($r_S = 0.1$ μm or $r_L = 1.0$ μm) and the initial volume fraction ($\phi_S = 1\%$ (circles), $\phi_S = 0.1\%$ (stars), and $\phi_L = 1\%$ (squares)). The evaporation rate is measured as ~ 0.3 nl s^{-1}, consistent with the estimate for decalin droplets [15].

($r_L = 1.0$ μm, $\phi_L = 1\%$: movie 3 [15]). Here the contact radius of a pure decalin droplet on a clean glass shows a good fit with an equation of $R(t) = R_0 t^{1/10}(1 - t/t_f)$ in Fig. 1(c) (solid line) where $R_0 t^{1/10}$ indicates classical spreading dynamics at early times (Tanner's law [16]) and $(1 - t/t_f)$ implies shrinkage dynamics by evaporation at late times [2]. This result is consistent with pure water on a clean mica surface [2]. We note that Tanner's law is considered as a universal law under complete wetting conditions [17]. Therefore, we conclude that the pure decalin droplet initially tends to completely spread on a glass surface.

Spreading is an intrinsic process for a pure fluid droplet gently placed on a homogeneous solid surface and is nearly independent upon early drying kinetics. Spreading of a pure fluid on a solid surface is generally described in terms of the "spreading coefficient" S, given by $S = \sigma_{sg} - \sigma_{sl} - \sigma_{lg}$, where σ is the respective interfacial tension between the solid-gas (σ_{sg}), solid-liquid (σ_{sl}), and liquid-gas (σ_{lg}) phases [5,6]. An equilibrium force balance at a three-phase contact line is described by Young's equation as $\sigma_{sg} = \sigma_{sl} + \sigma_{lg}\cos\theta_e$ with an equilibrium contact angle θ_e. Complete wetting ($\theta_e = 0$) is possible only when $S \geq 0$ [4,5]. Most molecular liquids show complete wetting on high-energy surfaces such as glass and metal [4]. Here we get a spreading (complete wetting) condition for pure liquids as $S \geq 0$. It is conceivable that if "spreading inhibition" is induced by particle confinement at an apparent contact angle ($\theta > 0$), a "latent" spreading force would exist as $F_S = 2\pi RS$ along the contact line ($2\pi R$).

Generally, surface irregularity [1] and solute accumulation [2] are considered as main effects that initiate self-pinning. In Fig. 1(a), we observed no spreading and only self-pinning in colloidal droplets with small or large colloids, while considerable spreading in a pure decalin droplet without colloids on the same glass surfaces. This result suggests that surface irregularity is not a critical factor in our case because the same glass surfaces were used for both pure and colloidal droplets. Self-pinning is the basis of the dynamics of the contact angle as $\theta(t) = \theta_0(1 - t/t_f)$ and of the volume as $V(t) = V_0(1 - t/t_f)$, as fitted with $\theta_0 \approx 15°$, $V_0 \approx 0.5$ μl, and $t_f \approx 1700$ s [solid lines in Figs. 1(d) and 1(e)]. Such linear decreases in $\theta(t)$ and $V(t)$ corroborate contact-line self-pinning during evaporation [18], regardless of the particle size ($r_S = 0.1$ μm or $r_L = 1.0$ μm) and the initial volume fraction [$\phi_S = 1\%$ (circles), $\phi_S = 0.1\%$ (stars), and $\phi_L = 1\%$ (squares)]. The evaporation rate is measured as ~ 0.3 nl s^{-1} for self-pinned droplets from the slope [Fig. 1(e)]. This measurement is consistent with the estimate of 0.29 nl s^{-1} [15] for self-pinned droplets from Hu-Larson's model [19]. The slow evaporation rate causes the slow radial flow velocity ($\mu < 1$ μm at 10 μm far from the contact line [15]), forming polycrystalline structures near the contact line (Fig. 2), similar to other results [20,21]. Therefore, solute accumulation is not expected to induce self-pinning by

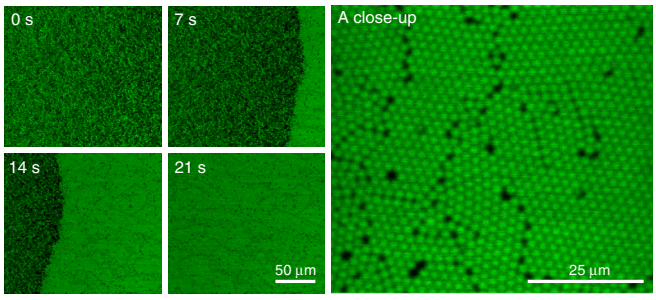

FIG. 2 (color online). High-resolution confocal images for a droplet with large colloids ($r_L = 1$ μm, $\phi_L = 5\%$) show that the particles form polycrystalline structures near the contact line. This result would be due to the slow evaporative flow rate.

such slow evaporative flows. As a result, surface irregularity [1] and solute accumulation [2] are ruled out as main effects to initiate self-pinning in colloidal droplets on glass surfaces.

A possible source of self-pinning is capillary force by solute confinement at a contact line [7–9]. In a situation of colloidal particles confined along a contact line [Fig. 3(a)], the outermost particle at the contact line experiences a capillary force, given by $F_C = 2\pi r\sigma_{lg}(\cos\theta)^2$ (a product of the horizontal force component of $\sigma_{lg}\cos\theta$ and the reduced perimeter of $2\pi r\cos\theta$ [9]), where σ_{lg} is the surface tension of the liquid-vapor interface ($\sigma_{lg} = 31.0\ \mathrm{mN\,m^{-1}}$ for decalin [11,12]) in Fig. 3(b). The corresponding net capillary force, retarding the spreading force, is described as $F_{NC} = NF_C = 2\pi rN\sigma_{lg}(\cos\theta)^2$ where N is the number of particles at the contact line. A drag force is generated for a particle moving near the substrate by the outward evaporative flow [Fig. 3(b)]. This drag force is a product of a friction coefficient and total attractive forces between colloids and substrate and practically is estimated as $F_D = 6\pi r\eta\mu$ [9]. Here, η is the dynamic viscosity of the fluid ($\eta \approx 3 \times 10^{-3}$ Pa s for decalin [11]) and μ is the radial velocity of the evaporative flow [9]. For a single colloid in decalin, the drag force, estimated as $F_D \approx 10^{-14}$ N for $r \approx 1\ \mu$m and $\mu \approx 1\ \mu\mathrm{m\,s^{-1}}$, is significantly smaller than $F_C \approx 10^{-7}$ N.

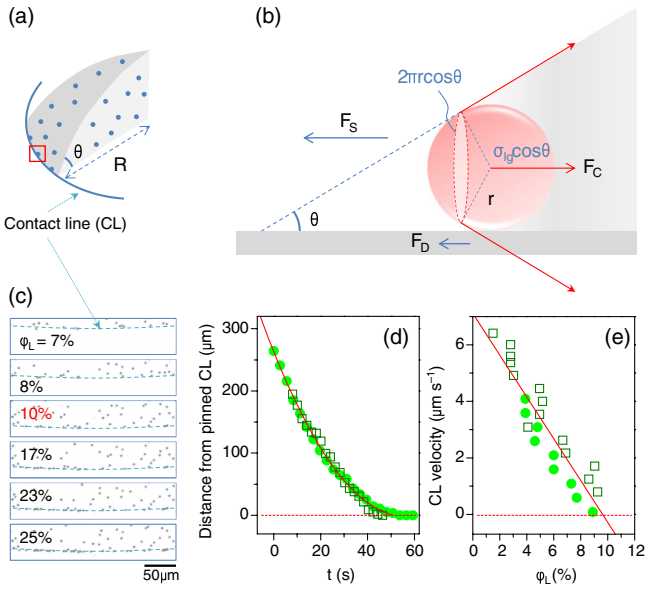

FIG. 3 (color online). Physical model and confocal observation for onset of self-pinning. (a) A pure droplet tends to complete wetting, implying a "latent" spreading force as $F_S = 2\pi RS$ along the contact line, where S is the spreading coefficient. The solute confinement inhibits the initial spreading. (b) The solute confinement induce a capillary force $F_C = 2\pi r\sigma_{lg}(\cos\theta)^2$ which is a product of the horizontal force component ($\sigma_{lg}\cos\theta$) and the reduced perimeter ($2\pi r\cos\theta$). A drag force F_D is significantly smaller than F_C. (c) Confocal observation of a critical linear packing fraction ($\varphi_L{}^*$) from a colloidal droplet ($V_0 = 0.5\ \mu$L and $\theta_0 = 15°$ with colloids of $r_L = 1.0\ \mu$m and $\phi_L = 1\%$). The contact line initially moves at $\varphi_L < \varphi_L{}^*$ and stops at $\varphi_L{}^* \approx 10\%$ and even at $\varphi_L > \varphi_L{}^*$. (d) The distance ($L$) from pinned contact line with time for large colloids (circles: movie 4 in the Supplemental Material [15]) and a bi-dispersed mixture (squares: movie 5 [15]). The CL velocity (v) was obtained from $v = -dL/dt$, where L was fitted by a quadratic form (solid line). (e) The φ_L dependence of the CL velocity. This analysis confirms $\varphi_L{}^*$ to be ~10% at $v = 0$.

We find a simple criterion of self-pinning at a contact angle ($\theta \neq 0$) by equating the net capillary force (F_{NC}) with the spreading force (F_S). Here, we define a linear packing fraction of particles (φ_L) at a contact line as $\varphi_L = 2rN/(2\pi R) = rN/\pi R$. The equality of $F_S = F_{NC}$ or $RS = rN\sigma_{lg}(\cos\theta)^2$ is immediately simplified as

$$\varphi_L = \frac{S}{\pi\sigma_{lg}(\cos\theta)^2}.$$

This criterion implies that the apparent contact angle depends only on the linear packing fraction at fixed S and σ_{lg}. This explains the same contact angles regardless of the particle size and the initial volume fraction, as illustrated in Fig. 1(d).

Our theory suggests the existence of a critical linear packing fraction ($\varphi_L{}^*$) at a contact line, when a colloidal droplet gets pinned at a critical contact angle (θ^*). We measured the critical value for a decalin droplet ($V_0 = 0.5\ \mu$l and $\theta_0 = 15°$) containing PMMA colloids ($r_L = 1.0\ \mu$m and $\phi_L = 1\%$) on a clean glass using confocal microscopy. An example series of snapshots taken by a real-time confocal imaging of a spreading front [Fig. 3(c)] shows that the contact line initially moves at $\varphi_L < \varphi_L{}^*$ and stops at $\varphi_L{}^* \approx 10\%$ and even at $\varphi_L > \varphi_L{}^*$. From two different samples (Supplemental Material, movie 4 for large colloids and movie 5 for a mixture of small and large colloids) [15], we measured the contact line velocity (v) from $v = -dL/dt$ where L is the front position far from the pinned contact line. Here, L decreases with time [Fig. 3(d)] while φ_L increases with time [Fig. 3(c)]. Despite different initial conditions, a good agreement is found in Fig. 3(e), showing that v decreases with φ_L. This analysis confirms $\varphi_L{}^*$ to be ~10% at $v = 0$. The dynamics in φ_L confirms the same critical condition for self-pinning to be $\varphi_L{}^* \approx 10\%$.

The value of $\varphi_L{}^* \approx 10\%$ suggests the existence of $\theta^* \approx 15°$, which determines the final drop diameter, regardless of particle diameter (d) and initial packing fraction (ϕ). To confirm this possibility, we fixed the initial drop volume ($V_0 \sim 0.7\ \mu$l) and then measured the drop diameter after evaporation with confocal microscopy [Fig. 4(a)] from a lot of various samples with different d (0.2, 0.7, 0.9, 1.0, 2.0, and 3.6 μm) and ϕ (0.1% ~ 50%). From a spherical cap model [Fig. 4(b)], we estimated the drop contact angle for each sample [Fig. 4(c)] as a function of the particle diameter (left) and the packing fraction (right). These data

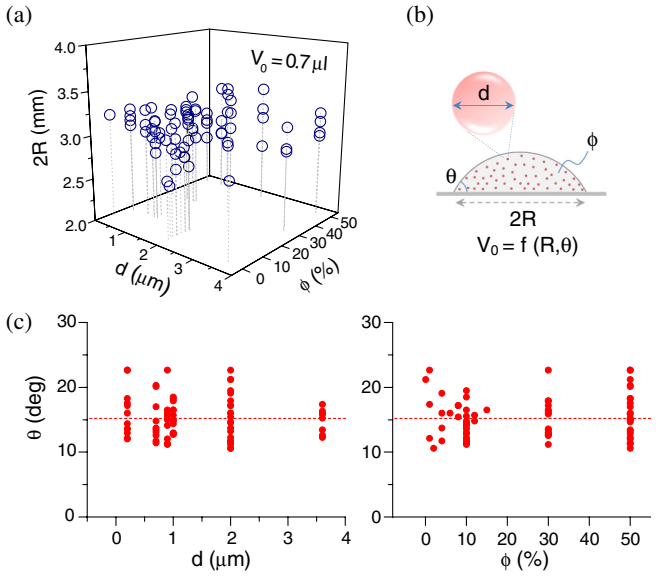

FIG. 4 (color online). (a) At a fixed initial drop volume ($V_0 \sim 0.7\ \mu$l), the drop diameter ($2R$) after evaporation was measured with confocal microscopy for different particle diameter ($d = 0.2$, 0.7, 0.9, 1.0, 2.0, and 3.6 μm) and packing fraction ($\phi = 0.1\% \sim 50\%$). (b) A spherical cap model is used to estimate θ from V_0 and R. (c) The drop contact angle as a function of d (left) and ϕ (right) suggests that the average contact angle is 15.2° (dashed lines), which agrees with our theory ($\theta^* \approx 15°$ for $\varphi_L{}^* \approx 10\%$).

suggest that the average contact angle is 15.2°, which agrees with our theory ($\theta^* \approx 15°$ for $\varphi_L{}^* \approx 10\%$).

We find an excellent agreement between the critical linear packing fraction of colloids for the onset of self-pinning and the experimental result taken by directly tracking individual particles. The contact-line pinning kinetics can be affected by many profound effects. These colloids are initially fully immersed in oil in terms of interfacial energies [14,22] and contribute to a dynamic pinning situation [Fig. 3(b)]. They are concentrated at the contact line as the contact angle rapidly decreases during spreading [23,24]. This situation would be helpful for the particle confinement at the contact line by reducing the interfacial energy between immiscible fluids [25,26] (such as air and decalin). From the estimate of $F_S = 2\pi RS \approx 10^{-5}$ N for $R = 1.4$ mm [14], the line tension effect (typically $\approx 10^{-10}$ N [27]) would be not significant. A shear force may be driven by evaporative flux but would not be significant at small contact angles [28]. For micro- and nanoparticles at the same volume fraction, because the total number of nanoparticles is much larger than that of microparticles, nanoparticles can get closer to the contact line, which may facilitate much easier self-pinning than microparticles [9]. This implies that nanoparticles can instantly bind to the contact line and build the initial ring width at $t \rightarrow 0$ (see discussion in Ref. [15]). Other effects such as particle ordering [20], jamming [2,29], and moving contact lines [30] would affect the contact-line pinning kinetics. Polymer grafting on the colloidal particles can make smaller particles more easily jammed [31]. Further experiments are required to understand various colloidal systems with different hydrophobicity.

In conclusion, to account for solute-induced self-pinning, we suggest a self-pinning mechanism based on spreading inhibition by solute confinement and find a critical linear packing fraction at a contact line. The critical condition is directly measured by microscopic observation with confocal microscopy. Our findings will help understand and control the coffee-ring-related effects of colloidal fluids for applications of printing and painting to fabricate organic devices, solar cells, and sensors or to perform biological and pharmaceutical tasks [32,33]. The solute-induced self-pinning has important implications in soft-matter physics, interfacial and colloid chemistry, nanoparticle-based fabrication, and nanofluids.

We thank David Weitz for confocal microscopy experiments at Harvard University. This research was supported by the Creative Research Initiatives (Functional X-ray Imaging) of MEST/NRF.

*bmweon@hotmail.com
†jhje@postech.ac.kr

[1] R. D. Deegan, O. Bakajin, T. F. Dupont, G. Huber, S. R. Nagel, and T. A. Witten, Nature (London) **389**, 827 (1997).
[2] R. D. Deegan, Phys. Rev. E **61**, 475 (2000).
[3] B. J. Fischer, Langmuir **18**, 60 (2002).
[4] P. G. de Gennes, Rev. Mod. Phys. **57**, 827 (1985).
[5] D. Bonn, J. Eggers, J. Indekeu, J. Meunier, and E. Rolley, Rev. Mod. Phys. **81**, 739 (2009).
[6] D. T. Wasan and A. D. Nikolov, Nature (London) **423**, 156 (2003).
[7] A. S. Sangani, C. Lu, K. Su, and J. A. Schwarz, Phys. Rev. E **80**, 011603 (2009).
[8] B. M. Weon and J. H. Je, Phys. Rev. E **82**, 015305 (2010).
[9] V. H. Chhasatia and Y. Sun, Soft Matter **7**, 10 135 (2011).
[10] H. Bodiguel and J. Leng, Soft Matter **6**, 5451 (2010).
[11] J. Leng, Phys. Rev. E **82**, 021405 (2010).
[12] J. S. Lee, B. M. Weon, S. J. Park, J. H. Je, K. Fezzaa, and W.-K. Lee, Nat. Commun. **2**, 367 (2011).
[13] A. Schofield, http://www.ph.ed.ac.uk/~abs/.
[14] B. M. Weon, J. S. Lee, J. T. Kim, J. Pyo, and J. H. Je, Curr. Opin. Colloid Interface Sci. **17**, 388 (2012).
[15] See Supplemental Material at http://link.aps.org/supplemental/10.1103/PhysRevLett.110.028303 for additional discussion and movie files.
[16] L. H. Tanner, J. Phys. D **12**, 1473 (1979).
[17] F. G. Wolf, L. O. E. dos Santos, and P. C. Philippi, J. Stat. Mech. (2009) P06008.
[18] B. M. Weon, J. H. Je, and C. Poulard, AIP Adv. **1**, 012102 (2011).
[19] H. Hu and R. G. Larson, J. Phys. Chem. B **106**, 1334 (2002).
[20] A. G. Marin, H. Gelderblom, D. Lohse, and J. H. Snoeijer, Phys. Rev. Lett. **107**, 085502 (2011).
[21] C. Monteux and F. Lequeux, Langmuir **27**, 2917 (2011).
[22] W. A. Goedel, Europhys. Lett. **62**, 607 (2003).

[23] E. Rio, A. Daerr, F. Lequeux, and L. Limat, Langmuir **22**, 3186 (2006).
[24] B. Berteloot, A. Hoang, A. Daerr, H. P. Kavehpour, F. Lequeux, and L. Limat, J. Colloid Interface Sci. **370**, 155 (2012).
[25] E. M. Furst, Proc. Natl. Acad. Sci. U.S.A. **108**, 20 853 (2011).
[26] D. M. Kaz, R. McGorty, M. P. Brenner, and V. N. Manoharan, Nat. Mater. **11**, 138 (2012).
[27] A. Checco, P. Guenoun, and J. Daillant, Phys. Rev. Lett. **91**, 186101 (2003).
[28] H. Gelderblom, O. Bloemen, and J. H. Snoeijer, J. Fluid Mech. **709**, 69 (2012).
[29] A. Liu and S. R. Nagel, Nature (London) **396**, 21 (1998).
[30] J. Zhou, B. Dupuy, A. L. Bertozzi, and A. E. Hosoi, Phys. Rev. Lett. **94**, 117803 (2005).
[31] V. Trappe, V. Prasad, L. Cipelletti, P. N. Segre, and D. A. Weitz, Nature (London) **411**, 772 (2001).
[32] M. Shih, H. M. Haverinen, P. Dhagat, and G. E. Jabbour, Adv. Mater. **22**, 673 (2010).
[33] P. J. Yunker, T. Still, M. A. Lohr, and A. G. Yodh, Nature (London) **476**, 308 (2011).